Max-Planck-Institut für Meteorologie

REPORT No. 321

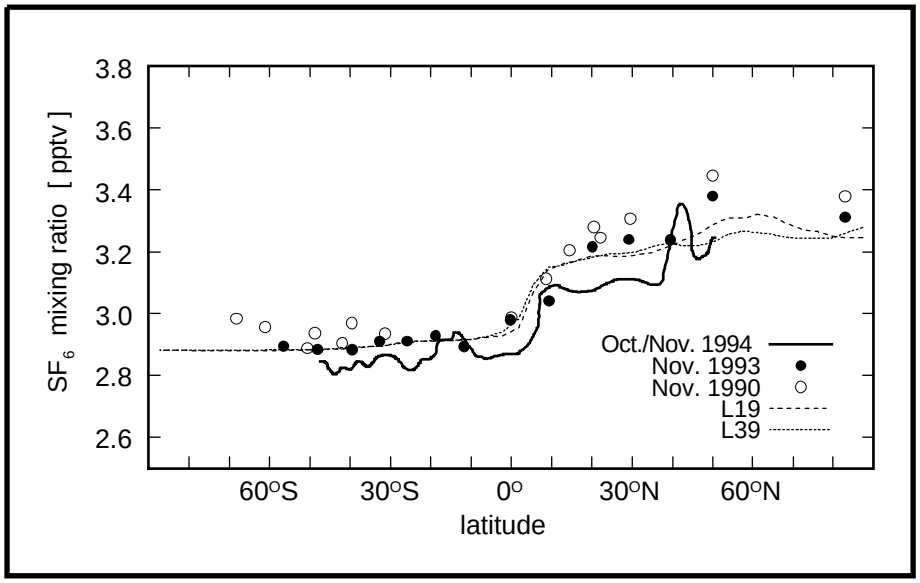

IMPACT OF THE VERTICAL RESOLUTION ON THE TRANSPORT OF PASSIVE TRACERS IN THE ECHAM4 MODEL

by

Christine Land • Johann Feichter • Robert Sausen

HAMBURG, June 2001

AUTHORS:

Christine Land
Johann Feichter

Max-Planck-Institut
für Meteorologie

Robert Sausen

Institut für Physik der Atmosphäre,
DLR Oberpfaffenhofen,
D- 82234 Wessling,
Germany

MAX-PLANCK-INSTITUT
FÜR METEOROLOGIE
BUNDESSTRASSE 55
D - 20146 HAMBURG
GERMANY

Tel.: +49-(0)40-4 11 73-0
Telefax: +49-(0)40-4 11 73-298
E-Mail: <name> @ dkrz.de

Impact of the Vertical Resolution on the Transport of passive Tracers in the ECHAM4 Model

C. Land[1*], J. Feichter[1], and R. Sausen[2]

[1]Max–Planck–Institut für Meteorologie, Bundesstraße 55,
D–20146 Hamburg, Germany,
[2]Institut für Physik der Atmosphäre, DLR Oberpfaffenhofen,
D–82234 Wessling, Germany

July 11, 2001
(submitted to Tellus)

ISSN 0937-1060

*Corresponding author's email address: land@dkrz.de

Abstract.

The transport of the passive tracers $^{14}CO_2$ and SF_6 has been modelled with two versions of the general circulation model ECHAM4 with different vertical resolution: the standard model with 19 model layers (L19) and a higher resolution version with 39 layers (L39). We study the impact of vertical resolution on the modelled transport characteristics. Both models are able to capture the observed SF_6 concentrations in the troposphere, but in the stratosphere the SF_6 mixing ratios are overestimated. L39 generally calculates higher stratospheric SF_6 mixing ratios than L19, and this deviation increases with altitude. The difference between the modelled profiles is partly attributed to the residual mean meridional circulation, which is stronger in L39 than in L19 and partly to the initial globally constant SF_6 concentration. The comparison of modelled $^{14}CO_2$ surface concentrations and vertical profiles with observations has shown that an increased vertical resolution in the climate model ECHAM4 reduces the strength of stratosphere troposphere exchange. L39 allows a better representation of sharp gradients at the tropopause than L19. This results in a weaker downward transport across the tropopause. However, compared to observations the downward transport is too strong also in the L39 simulation.

1 Introduction

The global model ECHAM4 has been established as a powerful tool for global climate variability and change simulations (e.g., *Sausen et al.*, 1997; *Roeckner et al.*, 1999) for climate sensitivity experiments (e.g., *Feichter and Lohmann*, 1997), and for tracer transport studies (e.g., *Timmreck et al.*, 1999; *Kjellström et al.*, 2000). However, characteristic shortcomings have shown up concerning the transport of chemical species and passive tracers in the model's stratosphere and upper troposphere. *Timmreck et al.* (1999), who modelled the eruption of the volcano Mount Pinatubo and the subsequent transport of volcanic aerosol, have shown that sulphate is transported poleward and downward into the model's troposphere at a rate much faster than observed. *Kjellström et al.* (2000) supported this finding in their transport study of $^{14}CO_2$, the oxidant of radiocarbon (^{14}C). They simulated the spreading of $^{14}CO_2$, which was introduced into the stratosphere of the northern hemisphere by above–ground nuclear weapon tests in the fifties and in the beginning of the sixties. They found that the modelled $^{14}CO_2$ concentration at surface stations increases faster than observed during the first year after the nuclear test ban treaty.

Insufficient vertical and horizontal resolution may be blamed for a substantial part of the deficient transport characteristics in the ECHAM4 model studies cited above. Sharp gradients, as they are observed for dynamic parameters like e.g., potential vorticity close to the tropopause, cannot be reproduced with the large grid box sizes typical for current GCMs. Additionally, the numerical diffusion associated with the semi–Lagrangian transport scheme used for the tracer transport is probably too strong. Enhanced spatial resolution can be expected to decrease the problems in either respect (*Rasch and Lawrence*, 1998).

So far efforts in improving large–scale dynamics have mainly focussed on increasing the horizontal resolution (e.g., *Boville*, 1991; *Senior*, 1995; *Williamson et al.*, 1995; *Marshall et al.*, 1997), developing more sophisticated parametrisation schemes (e.g., *Lohmann and Roeckner*, 1996), or different transport schemes (e.g., *Rasch and Lawrence*, 1998; *Reithmeier and Sausen*, 2001). Only little attention has been paid to the sensitivity of simulated dynamics on the vertical resolution, although *Lindzen and Fox-Rabinovitz* (1989) explained that the vertical resolution has to be chosen dynamically consistent to the horizontal resolution in order to improve the quality of the model output. Their findings were supported by *Olga et al.* (1991). Also *Tsuyuki* (1994) showed that a higher vertical resolution in the stratosphere is necessary to improve the simulated tropospheric variability. However, *Boville* (1991) detected only minor changes as he reduced the vertical grid spacing from 2.8 to 0.7 km at a horizontal spectral resolution of T21. *Tompkins and Emanuel* (2000) pointed out that GCMs need a vertical resolution of at least 25 hPa to attain numerical convergence in simulated water–vapour distribution.

The impact of the horizontal and vertical resolution on simulated climate statistics has already

been studied with ECHAM4.L19 (hereafter abbreviated L19) and ECHAM4.L39(DLR) (hereafter referred to as L39), a version of ECHAM4 with higher vertical resolution (*Stendel and Roeckner*, 1998; *Land et al.*, 1999, respectively). However, it had not yet been examined how sensitive the tracer transport in ECHAM4 is to an increased vertical resolution. *Austin et al.* (1997) were able to improve the ozone distribution in their GCM simulations by increasing the number of vertical levels from 19 to 49 mainly in the tropopause region. *Pope et al.* (2001) substantially improved the simulated water vapour and temperature distribution in the Hadley Centre Climate model by increasing the number of model layers from 19 to 30. In this study we use the passive tracers sulphur hexafluoride (SF_6) and excess $^{14}CO_2$, namely $^{14}CO_2$ which was introduced into the atmosphere by above–ground nuclear weapon tests, to assess the impact of an increased vertical resolution on the simulated tracer transport.

SF_6 and excess $^{14}CO_2$ are valuable tracers for atmospheric and hydrologic dynamics, because they are very stable and can be measured with high accuracy (*Hesshaimer et al.*, 1994; *Maiss et al.*, 1996; *Upstillgoddard and Wilkins*, 1998). SF_6 is an anthropogenic trace gas with a lifetime of about 3200 years. It is predominantly used as an insulating gas in high voltage electrical equipment, but also as a cover gas in the metal processing industries. It escapes to the atmosphere through leaks and during repair or servicing (*Ko et al.*, 1993). SF_6 has already been used to evaluate model dynamics in terms of stratosphere–troposphere exchange (*Kjellström et al.*, 2000) and transport time scales (*Manzini and Feichter*, 2000; *Waugh et al.*, 1997) and to compare the transport characteristics of several global models (*Denning et al.*, 1999). The radioactive isotope carbon–14 (^{14}C) is naturally produced by interaction of neutrons with atmospheric nitrogen in the upper atmosphere. However, due to the above–ground nuclear weapon tests of the late 1950s and 1960s the atmospheric ^{14}C level was increased substantially. In 1963 the northern hemisphere surface concentration was twice the background value (*Nydal and Lövseth*, 1983). ^{14}C has a half–life of 5730 years. In the atmosphere it is rapidly oxidised to form $^{14}CO_2$ which is incorporated in the global carbon cycle. ^{14}C has been used to study stratosphere dynamics in 2D models (e.g., *Johnston*, 1989; *Kinnison et al.*, 1993; *Shia et al.*, 1993) and to analyse the carbon exchange between the atmosphere and the oceans (e.g., *Hesshaimer et al.*, 1994).

2 Model description

The global model ECHAM4 was developed from the weather forecast model of the European Centre for Medium–Range Weather Forecasts (ECMWF). It is a spectral model based on the primitive equations. The prognostic variables are the logarithm of surface pressure, temperature, vorticity and divergence of the horizontal wind, water vapour, and liquid water mixing ratio. In addition a number of passive tracers can be transported. Water vapour, cloud wa-

ter, and tracers are advected by a semi–Lagrangian scheme (based on *Williamson and Rasch*, 1989, 1994) while the remaining prognostic variables are transported by the Eulerian (spectral) advection scheme. A horizontal spectral resolution of T30 is used for the current study, corresponding to an isotropic resolution of about 6° for dynamics. The semi–Lagrangian scheme and the parametrised physical processes are calculated on the associated Gaussian transform grid of approximately $3.75° \times 3.75°$ in latitude and longitude. The semi–implicit leap–frog time stepping scheme employs a time step of 30 minutes. The model contains a state of the art parametrisation package for unresolved dynamical and physical processes, including radiation, cumulus convection, stratiform clouds, gravity wave drag, vertical turbulent diffusion and surface fluxes, land surface processes, and horizontal diffusion. The characteristics of the ECHAM4 standard model are described comprehensively by *Roeckner et al.* (1996), and ECHAM4 features that were adopted from previous ECHAM versions or from the original ECMWF forecast model can be found in *Roeckner et al.* (1992) and *Simmons et al.* (1989), respectively.

The atmosphere general circulation model L39 was derived from the operational ECHAM4 model. While the standard ECHAM4 uses 19 vertical levels, L39 vertically resolves the model atmosphere with 39 layers in a hybrid σ–p coordinate system (see Figure 1). The top layer of both models is centred at 10 hPa (about 30 km). The highest increase in vertical levels has been achieved in the upper troposphere and above, e.g. the layer depth in the tropopause region has been reduced from 2.0 to 0.7 km. L39 was tuned independently from the 19 layer version in order to account for the effect of parametrisations that depend on the layer thickness like the cloud scheme.

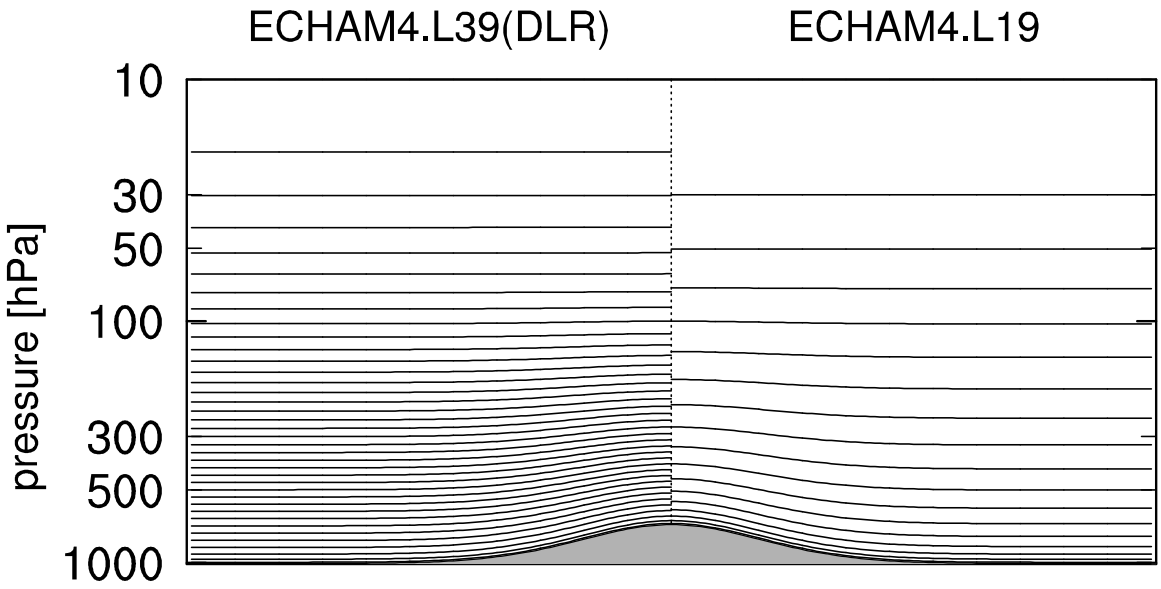

Figure 1: Distribution of the model levels in ECHAM4.L39(DLR) (left) and ECHAM4.L19 (right) for a reference surface pressure of 1013 hPa and an idealized orography.

Land et al. (1999) provide a detailed model description and compare the main features of the climatologies simulated with both model versions at T30 horizontal spectral resolution. Only a few variables are sensitive to a change in vertical resolution: cloud coverage is significantly reduced in L39, particularly in the upper troposphere, and the variability of temperature and zonal wind on daily and weekly time scales is substantially enhanced above 50 hPa.

3 Simulation set–up

The objective of this paper is to determine the impact of an increased vertical resolution on the transport and distribution of passive tracers. Therefore numerical experiments have been performed with L39 and L19 simulating the distributions of $^{14}CO_2$ and SF_6. The modelled tracer set–up is outlined in this section.

3.1 SF_6

SF_6 is initialised in both models with a globally uniform concentration field of 2.06 pptv on January 1, 1989 according to *Denning et al.* (1999). The period 1989 to 1993 (five years) is then simulated by running the model in climatological mode with observed sea surface temperatures and ice cover as boundary conditions. The surface emission flux of SF_6 is prescribed using estimates of monthly global emissions rates as proposed by *Levin and Hesshaimer* (1996). The SF_6 sources and their strength are distributed geographically according to population density and electrical power usage as given in *Denning et al.* (1999) (see Figure 2). SF_6 is predominantly

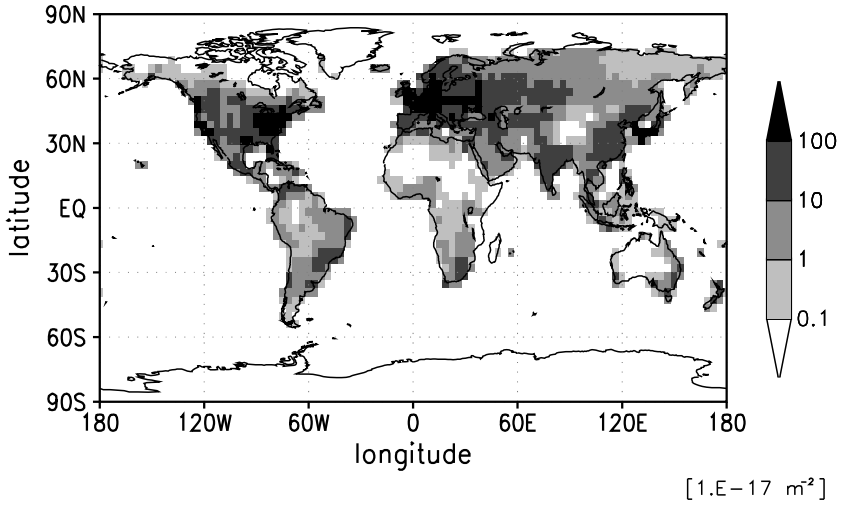

Figure 2: Geographical distribution and density of SF_6 sources.

emitted in industrialised regions of the northern hemisphere, such as North America, Europe,

and South East Asia. There are no sinks in the troposphere and stratosphere. *Ravishankara et al.* (1993) assume that SF_6 is destructed in the mesosphere as a results of electron attachment. As this sink is still very unclear, we did not include it in our model simulations. In the following, results with respect to SF_6 are presented from the last year of the model integration.

3.2 $^{14}CO_2$

Based on observed profiles of $^{14}CO_2$ *Johnston* (1989) constructed the zonally symmetric distribution of excess $^{14}CO_2$ for October 1963. This distribution represents only a rough estimate, because observations were scarce. Many injections occurred during the nuclear test series, and the total amount of radioactive material introduced is unclear. Error estimates for this distribution have not been given. In their recent study *Hesshaimer and Levin* (2000) systematically investigated the observational basis for this distribution, namely the stratospheric air samples collected during nuclear weapon tests and published in Health and Safety Laboratory reports. They determined an uncertainty of less than $\pm 5\%$ for the quarterly mean stratospheric $^{14}CO_2$ activity concentrations.

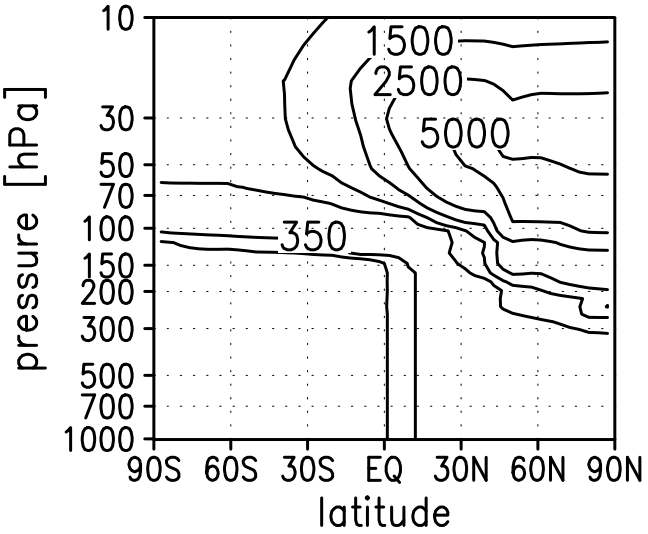

Figure 3: Zonal mean distribution of excess $^{14}CO_2$ volume mixing ratio as used as initial distribution for October 1963 in the L39 simulation. Isolines: 300, 350, 500, 850, 1500, 2500, and 5000×10^{-18} mole/mole.

As the transport in the stratosphere is dominated by zonal winds it is assumed that bomb introduced $^{14}CO_2$ is distributed zonally homogeneously nine months after the series of bomb tests. The zonal mean distribution of excess $^{14}CO_2$ has been transferred to the different model grids of L19 and L39 (see Figure 3). Excess ^{14}C was predominantly released into the stratosphere of the northern hemisphere. Maximum $^{14}CO_2$ volume mixing ratios there exceeded

5000×10^{-18} mole/mole poleward of 30°N between 100 and 50 hPa. In the troposphere of the southern hemisphere the $^{14}CO_2$ concentration was lower than 300×10^{-18} mole/mole.

The temporal variation of the tropospheric $^{14}CO_2$ concentration is determined by exchanges with the ocean, the terrestrial biosphere, and the upper atmosphere, which includes variations in the natural production, anthropogenic emissions, and radioactive decay. Following *Hesshaimer et al.* (1994) we apply a simple module for the global carbon cycle. We divide the biosphere into three carbon reservoirs (Figure 4). The smallest represents leaves, fine roots, and twigs. It has a capacity of 105 Pg(C) and its turnover time is 3 years. The second reservoir, with a capacity of 675 Pg(C) stands for branches, roots, and tree–trunks. It takes 27 years to fully replenish it. Soils store the largest amount of carbon. This reservoir is fed by both other reservoirs. It has a capacity of 1420 Pg(C) with a turnover time of 375 years. The $^{14}CO_2$ content of the oceans and the exchange with the terrestrial biosphere in the model depends on the $^{14}CO_2$ concentration at the surface level and the $^{14}CO_2$ content in each reservoir, and is proportional to the $^{12}CO_2$ surface fluxes as depicted in Figure 4. This simple model for the global carbon cycle only accounts for long-term exchanges between each reservoir. Seasonal variations are not included.

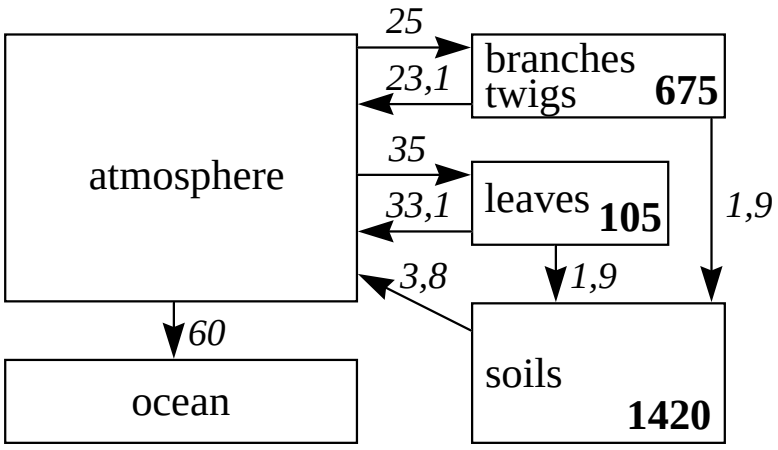

Figure 4: Global carbon cycle and $^{12}CO_2$ fluxes [Pg(C)/a] between the reservoirs together with selected reservoir sizes [Pg] as used in the model simulations.

In the model simulation only the distribution of excess $^{14}CO_2$, namely additional $^{14}CO_2$ from above–ground nuclear weapon tests is modelled. Therefore the natural production of $^{14}CO_2$ and the emission due to other anthropogenic sources (e.g., fossil fuel combustion or release from light water reactors) is omitted. Oceans are able to store a vast amount of carbon. It is assumed that dissolved $^{14}CO_2$ is rapidly mixed downward. Therefore the flux back from the ocean into the atmosphere is neglected. $^{14}CO_2$ has a radioactive half–life of 5730 years. As the $^{14}CO_2$–simulation period extends only over 10 years the radioactive decay of $^{14}CO_2$ is negligible.

4 Results and comparison with observations

4.1 SF_6

Surface values

The observed SF_6 mixing ratio at the surface closely follows a quadratic function in time (*Geller et al.*, 1997). The global trend of the modelled mixing ratio (in pptv) at the surface can be approximated by

$$\chi_0^{L39}(t) = 3.532 + 0.230\,t + 0.002\,t^2 \quad \text{for L39} \tag{1}$$

$$\chi_0^{L19}(t) = 3.527 + 0.226\,t + 0.001\,t^2 \quad \text{for L19} \tag{2}$$

with t being the time (in years) relative to 1996. The modelled monotonic increase is slightly faster than the growth rate that *Geller et al.* (1997) calculated from observational data. Using the same emission scenario *Denning et al.* (1999) also detected in their intercomparison study that the simulated surface mixing ratio was higher than observed for every model at all times of the year 1993 at all measurement sites. However, the differences between both curves remain small during this period: in the beginning of 1989 the modelled mixing ratio is lower than observed by 0.04 pptv, and in the end of 1993 it is about 0.06 pptv higher (see Fig. 5). Consequently, we are confident with the chosen emissions.

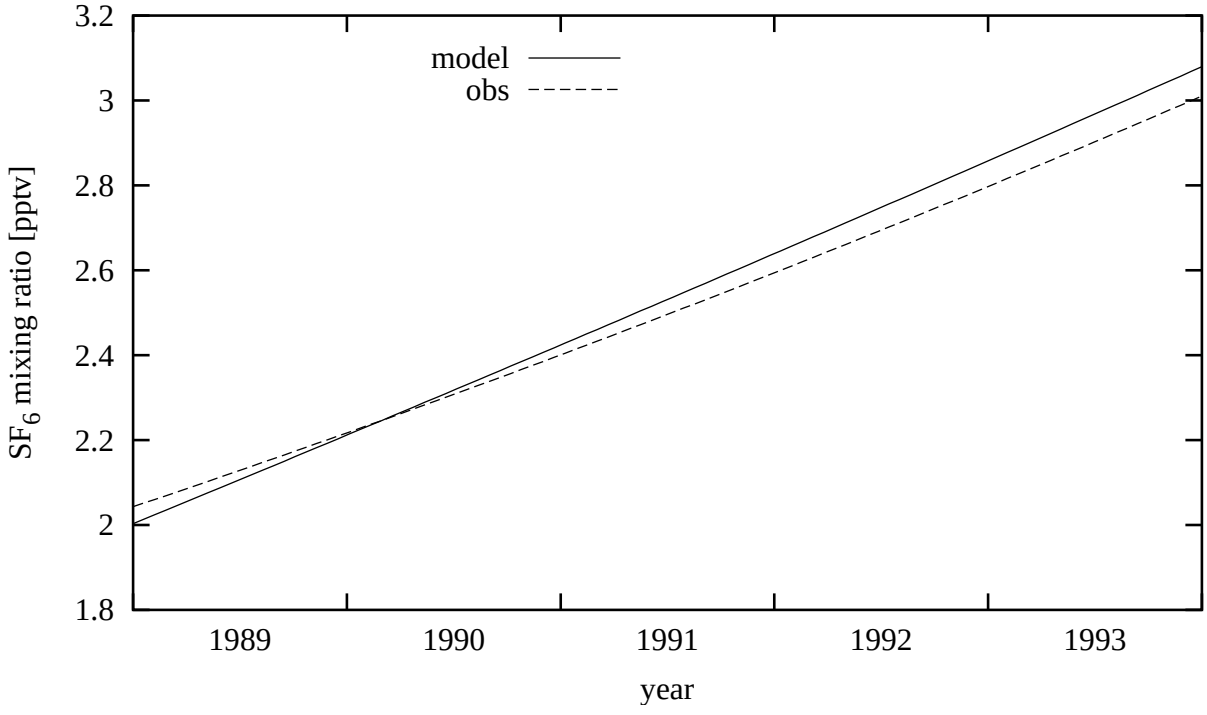

Figure 5: Observed and modelled (L39) increase of the SF_6 mixing ratio near the surface.

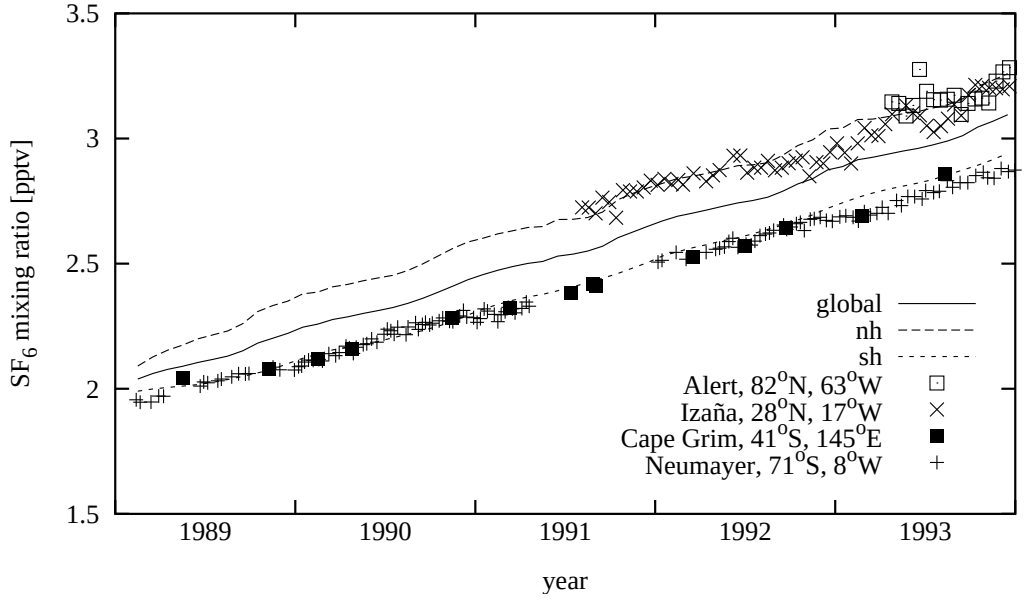

Figure 6: Observed and modelled SF_6 mixing ratios near the surface. The observations are taken at Alert (⊡), Izaña (×), Cape Grim (■), and at Georg von Neumayer (+). The curves represent global, northern hemisphere, and southern hemisphere, resp., means of the L39 model results.

In Figure 6 the observed and the modelled SF_6 increase near the surface are depicted. The differences between both model simulations are very small, i.e. lower than 0.02 pptv. Therefore only the model values from the L39 simulation are plotted. As SF_6 is predominantly emitted at the surface of the northern hemisphere, the mixing ratio there is higher than in the southern hemisphere. The values at Izaña (28°N, 17°W) and Georg-von-Neumayer station (71°S, 8°W) differ by about 0.3 pptv. These features are nicely captured by both model versions.

The geographical distribution of the SF_6 mixing ratio as simulated by L39 at the lowest model level for December 1993 is shown in Figure 7 together with the difference between both model simulations. The SF_6 mixing ratio is high above the source regions of both hemispheres. In the northern hemisphere it exceeds 3.6 pptv above the eastern United States, Europe, and Southeast Asia. Compared to the northern hemisphere concentrations near the surface the SF_6 distribution in the southern hemisphere is more zonally uniform, though the 3.2 pptv isoline bulges southward over South America and Africa. The differences between the two model simulations are confined to the regions with the highest emissions, but remain small, i.e., below 2% (Fig. 7, right).

Figure 8 displays meridional profiles of the surface SF_6 mixing ratio as modelled by L39 and L19 for November 1993 together with observations taken over the Atlantic Ocean in November 1993 and November 1990 by the University of Heidelberg (UOH) (*Levin and Hesshaimer*, 1996), and in November 1994 by NOAA. The latter data have been adjusted to the UOH calibration scale (*Geller et al.*, 1997). Additionally, all observational data have been scaled to November 1993

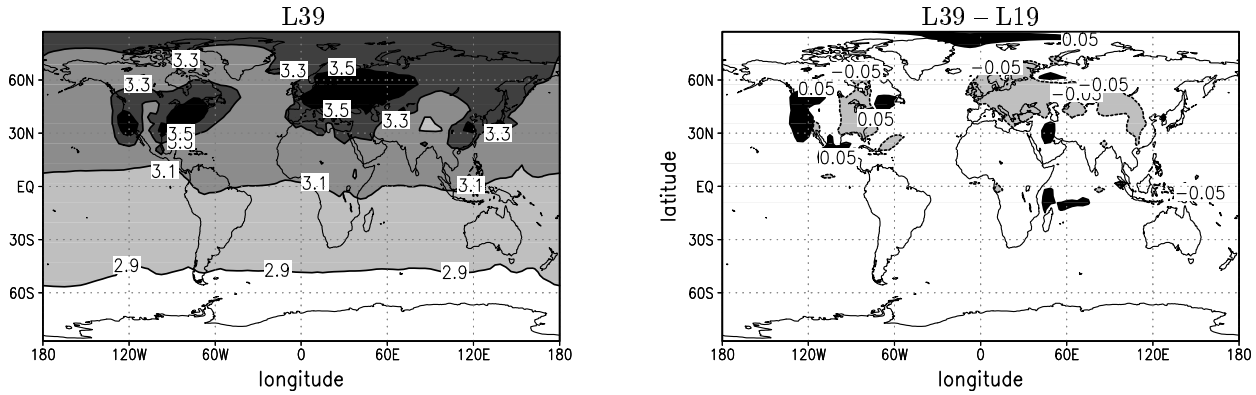

Figure 7: Monthly mean SF_6 mixing ratio near the surface as modelled by L39 (left) and difference between both model simulations (L39 – L19, right) for December 1993. Positive (negative) values are shaded in black (grey). Unit: pptv.

with the global growth rate as given by *Geller et al.* (1997). We used the global growth rate to scale the observational data. In the years before 1994, the difference between the global growth rate and the growth rates at the surface of the northern and the southern hemisphere was less than 1%. The SF_6 concentration would therefore only be marginally different if the hemispheric growth rates had been used to scale the data. Also in this graph the strong concentration gradient at the surface between the northern and the southern hemisphere is clearly visible. Compared to the observations both models realistically simulate this meridional profile. The model results differ only slightly in northern hemisphere mid-latitudes. However, it is not possible to say how significant this result is without running an ensemble of simulations, starting with differing meteorological conditions. We refrained from this due to the high computational expense.

On the whole, these results show that the geographical distribution of the sources and their strength are chosen appropriately to yield realistic surface concentrations in the model simulations. To estimate the global performance of both models, the vertical distribution has to be evaluated.

Vertical distribution and profiles

In Figure 9 the annual and zonal mean SF_6 distribution for 1993 as simulated by L39 and the difference between both model simulations are shown. In the L39 simulation (Fig. 9, left) the SF_6 mixing ratio decreases with increasing altitude. Ranging from more than 3.4 pptv at the surface of the northern hemisphere midlatitudes to values lower than 2.6 pptv poleward of 50°N above 50 hPa. Further, the SF_6 mixing ratio decreases monotonically from north to south in the whole troposphere. In the stratosphere, however, at a given altitude the concentration is greatest in the tropics and decreases towards the poles. This structure reflects the residual mean meridional circulation with tropospheric air entering the stratosphere in the

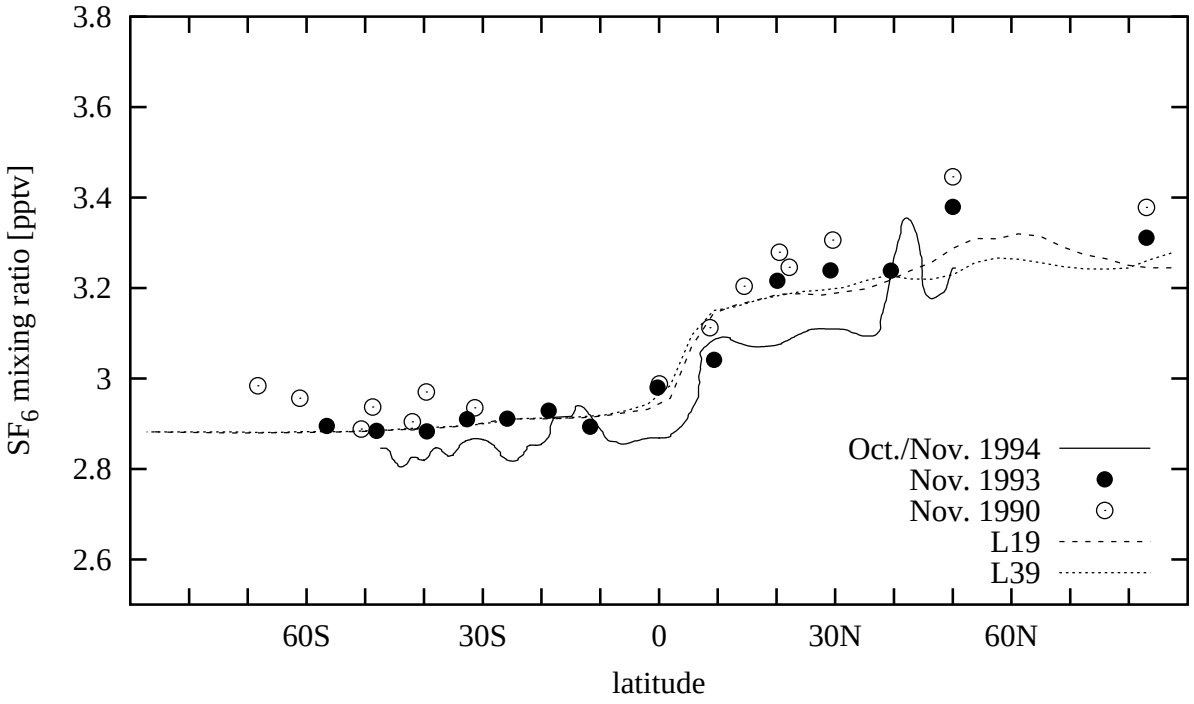

Figure 8: Meridional profiles of the surface SF_6 mixing ratio on the Atlantic Ocean as modelled by L39 (short dashed) and L19 in November 1993 (long dashed), and observed by UOH in November 1990 ($\odot$), and November 1993 ($\bullet$) (*Levin and Hesshaimer*, 1996), and by NOAA in October/November 1994 (straight line) (*Geller et al.*, 1997)).

tropics, rising upward, and moving poleward downward in higher latitudes (*Holton*, 1986). The difference between both model simulations is small in the troposphere (less than 1.5%), but in the stratosphere the model results differ systematically, especially in the northern hemisphere. Above the tropopause L39 simulates higher mixing ratios than L19, and the difference increases with altitude (Fig. 9, right). This difference can be explained by a stronger residual mean meridional circulation in the L39 simulation (see Figure 10). In the L39 simulation the northern hemisphere annual mean meridional mass circulation is significantly stronger than in the L19 model run. This can be attributed to the low-frequency variability of the meridional temperature transport, which is distinctly stronger in the uppermost model levels of the L39 simulation compared to L19 (see *Land et al.*, 1999). In the southern hemisphere both models give rather similar results with respect to the residual mean mass circulation.

In Figure 11 we show observed vertical profiles of the SF_6 mixing ratio from balloon soundings in Esrange (68°N), Aire sur l'Adour (44°N), and Hyderabad (17°N) (*Harnisch et al.*, 1996; *Patra et al.*, 1997) together with monthly mean results of both model simulations for December 1993 to evaluate both models. All observational vertical profiles have been scaled to December 1993. It has to be kept in mind that the reference growth rate is valid for the surface and not necessarily for the stratosphere. As the stratospheric concentration lags behind the tropospheric

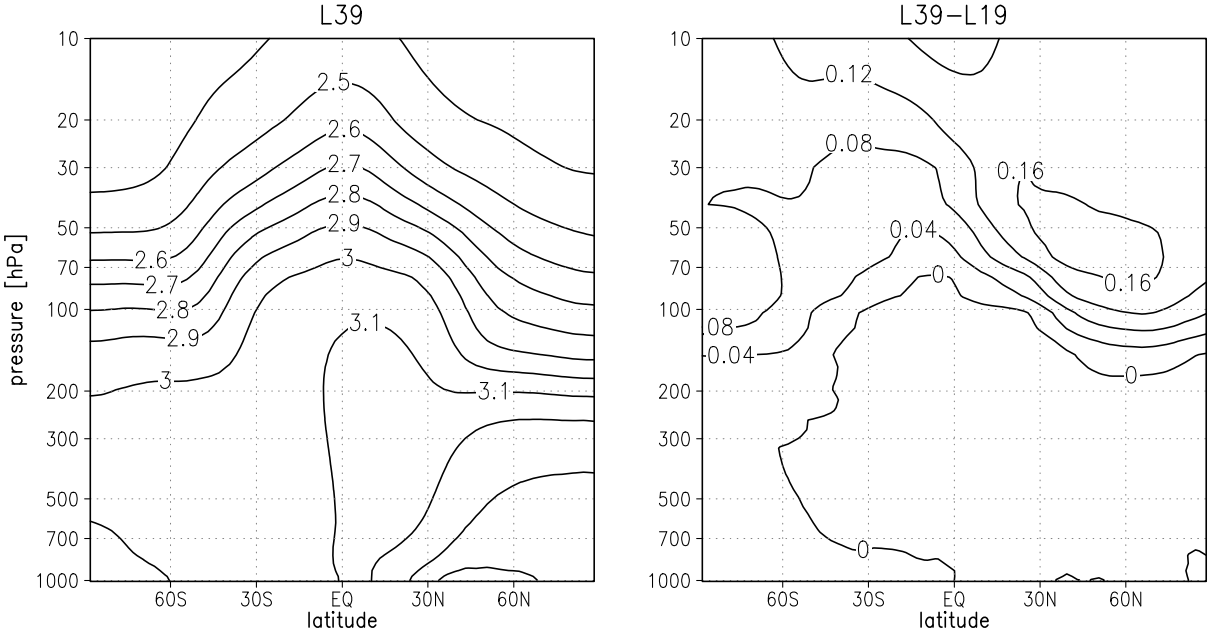

Figure 9: Annual and zonal mean SF_6 mixing ratios as modelled by L39 (left) and differ ence L39 minus L19 (right) for 1993. Unit: pptv.

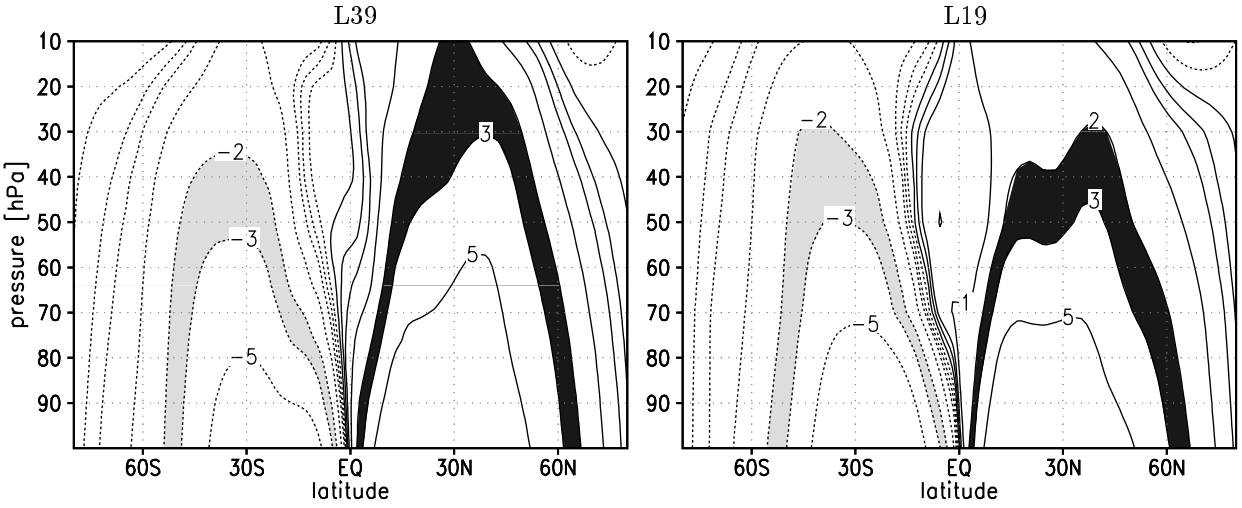

Figure 10: Annual mean residual mean meridional mass flux in units of 10^9kg/s as simulated by L39 (left) and L19 (right). Values between -3 to -2·10^9kg/s and 2 to 3·10^9kg/s are shaded in grey and black, respectively.

one, the scaling would be more accurate if the age of air had been taken into account. However, the difference is again small. A SF_6 concentration of 1.5 pptv in the stratosphere in January 1992 (e.g. at the station Esrange (see Figure 11)) would increase to 1.9 pptv until December 1993 using solely the surface growth rate. Taking an age of 4 years into account, the same concentration would rise to a slightly lower value of 1.8 pptv.

In general, model results and observations are in good accordance below the tropopause. How-

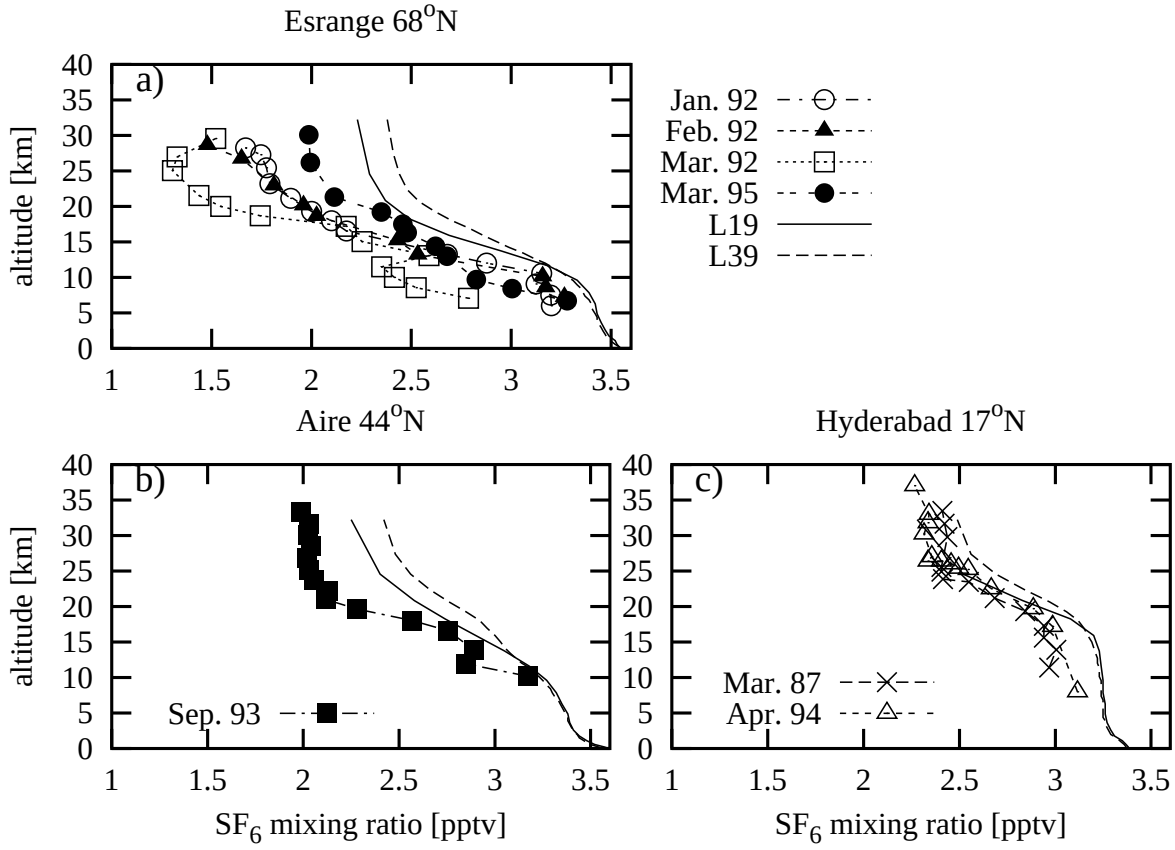

Figure 11: Observed profiles of the SF_6 mixing ratio adjusted to December 1993 at different locations.

ever, above the tropopause, especially in 44°N and 68°N (Fig. 11a,b) the model simulations give higher ($< 10\%$ in Aire) mixing ratios than observed. The difference between model and observational values is greatest inside the polar vortex. This deviation can mainly be attributed to the chosen initial SF_6 distribution. The model simulations were started with a globally uniform mixing ratio of 2.06 pptv. In 1993 the model values in the stratosphere have to exceed the initial mixing ratios, because the supply of SF_6 from the troposphere increases with increasing surface emissions. Therefore the model values in the stratosphere exceed the observed concentrations, which are lower or about the same value than the initial SF_6 mixing ratio. Further, the modelled horizontal diffusion might be somewhat too high at a spectral resolution of T30. Increasing the horizontal resolution would reduce the diffusion due to the semi–Lagrangian advection scheme (*Rasch and Williamson*, 1990). In Hyderabad (Fig. 11c) the agreement between observed and modelled profiles is rather good.

Mean age of the stratospheric air

As SF_6 does not have any sink in the stratosphere, the vertical structure of its mass mixing ratio, namely the decrease with increasing altitude, is dominated by the mass exchange rate between the troposphere and the stratosphere. The transport timescale of the exchange may

be described by the mean age of the air mass. The concept of age, taking into account the statistical nature of air parcels was formally developed by *Hall and Plumb* (1994). Based on their work, *Waugh et al.* (1997), *Hall and Waugh* (1998), and *Hall et al.* (1999) derived the mean age of stratospheric air from chemical transport model simulations. The mean age of an air mass in the stratosphere is the lag time of the stratospheric response from the tropospheric mixing ratio (*Schmidt and Khedim*, 1991). Given that the tracer concentration does not have any sink and the surface concentration increases linearly in time, the mean age Γ of an air mass at a location $\vec{r}$ with a tracer concentration $\chi(\vec{r},t)$ can be approximated by determining the time when the surface had the same concentration (*Waugh et al.*, 1997):

$$\chi(\vec{r},t) = \chi_0(t - \Gamma(\vec{r})) \tag{3}$$

The mean age Γ_S at a point $\vec{r}$ in the stratosphere is the time lag between the occurrence of the tracer concentration $\chi_S(\vec{r},t)$ at point $\vec{r}$ and the previous occurrence of this concentration at the equatorial tropopause (χ_{TP}):

$$\chi_S(\vec{r},t) = \chi_{TP}(t - \Gamma_S(\vec{r})) \tag{4}$$

In general, it takes a time $\delta\Gamma$ for the global mean signal of the surface tracer concentration to reach the equatorial tropopause. As the mean age in the stratosphere has been defined with reference to the equatorial tropopause, but will be calculated by using χ_0 (Eqs. (1) and (2) for L39 and L19, respectively), Γ_S has to be reduced by $\delta\Gamma$

$$\chi_S(\vec{r},t) = \chi_0(t - \Gamma_S(\vec{r}) - \delta\Gamma)\,. \tag{5}$$

SF_6 is a highly suitable tracer for calculating precisely the mean age: the emissions increase linearly, the gas is long–living, and the trend of the surface concentration is documented quite well. Its surface concentration increases quadratically in time. *Volk et al.* (1997) determined Γ_S for a quadratically increasing surface concentration of SF_6 and compared their results with those achieved assuming a linear increase. With a given SF_6 mixing ratio Γ_S is lower assuming linear increasing SF_6 mixing ratios. The time difference decreases with decreasing mixing ratio and therefore increases with increasing age of an air mass. However, the difference was only 0.5 years for the oldest air masses in their investigation (Γ_S = 6 years). From observational data *Volk et al.* (1997) determined $\delta\Gamma$ to be 0.8 a. The L39 and the L19 model simulate a lower value of 0.3 a and 0.4 a, respectively.

In the following, the structure of mean age in the stratosphere is determined using the results of the year 1993 by inverting Eq. (5) using Eqs. (1) and (2). Figure 12 depicts the vertical age structure of both models. In both model simulations the mean age is lowest in the lower tropical stratosphere. It increases poleward and with increasing altitude. Table 1 shows the meridional gradient of annual mean age between both poles and the tropics for the 50 and the 100 hPa level as modelled by L39, L19, and MAECHAM4. In 50 hPa it is about 2 years and in 100 hPa it is 1.5 and 2 years in the L39 and the L19 simulation, respectively.

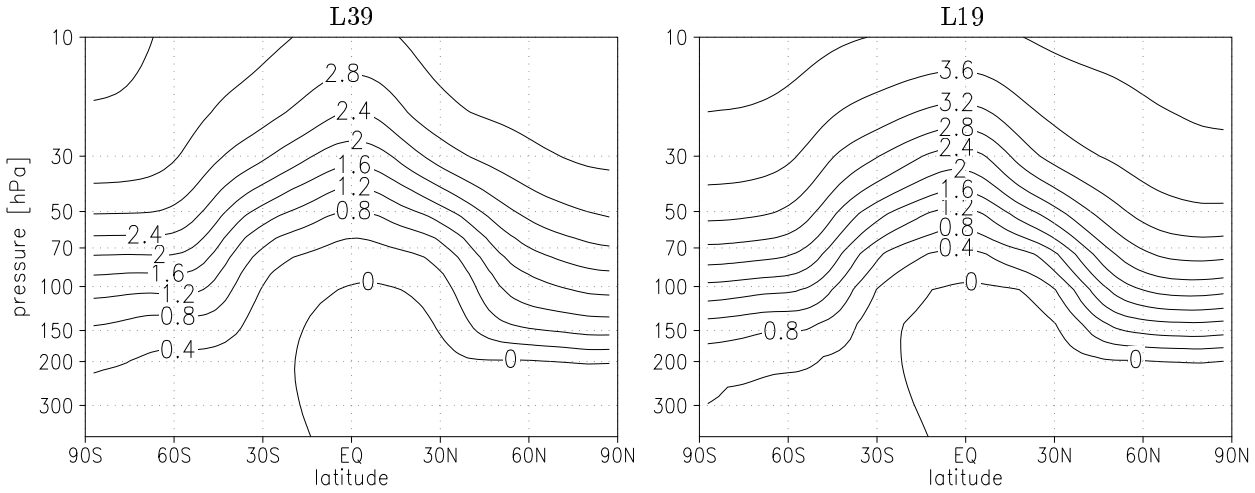

Figure 12: Vertical structure of the mean age as determined from simulations with L39 (left) and L19 (right). Unit: a.

Table 1: Meridional gradient of annual mean age [a] between the poles and the tropics for the 50 and the 100 hPa level as modelled by L39, L19, and MAECHAM4.

Model	100 hPa	50 hPa
L39	1.5	2.0
L19	2.0	2.0
MAECHAM4	2.0	2.5[(a)]

[(a)] Value is valid for the 54 hPa level.

These values agree with the age distribution of the GISS model (Goddard Institute for Space Studies' Global Climate Middle Atmosphere model) shown in *Hall and Waugh* (1997) (their Figure 1) and is slightly lower than the values achieved with the MAECHAM4, the middle atmosphere version of ECHAM4, whose top model level is centred at about 80 km. In the MAECHAM4 simulation the difference in annual mean age between the equator and the poles is about 2.5 years in 54 hPa and 2 years in 100 hPa (*Manzini and Feichter*, 2000). Using a CTM covering the atmosphere up to 50 km, *Waugh et al.* (1997) determined a meridional age gradient which was twice as large. The air mass in 20–30 km altitude (50–10 hPa) was 2 years older. The stratospheric age structure calculated from observed vertical SF_6–profiles also shows older air above the poles. *Harnisch et al.* (1996, 1998) determined an age of 5–10 years for air masses in the polar vortex. These high values might be attributed to air masses with low SF_6 mixing ratios coming from high altitudes and sinking downward above the poles. As the top levels of both of our model versions are centred at 10 hPa and no sink has been described, the mean age in the models has to be lower compared to these observations. Calculations from observations show that the mean age increases from 4 to 5 years with increasing latitude on the northern

hemisphere above 20 km (*Harnisch et al.*, 1996; *Patra et al.*, 1997). In the models presented here the age values are lower, indicating that horizontal mixing is overestimated. Furthermore, due to the homogeneous initial SF_6 distribution the horizontal concentration gradient between lower and higher latitudes might be underestimated, resulting in lower age values in the polar vortex.

In a more recent work *Hall and Waugh* (1998) showed that despite the long lifetime of SF_6 its chemical destruction in the mesosphere is relevant for the mean age calculation from observations. Due to this sink, the vertical concentration gradients are lower than they would be for a perfectly inert tracer. Therefore the observed mean age is overestimated. Thus, if the mesospheric sink had been included in the model simulations, the mean age would most likely agree better with the observations. *Hall and Waugh* (1998) found that the overestimation is higher in the extratropics than in the tropics. Depending on the model used and prescribed sinks the age in 68°N was overestimated up to 10% in 20 km and up to 65% in 30 km. Consistent with the results shown so far the vertical age gradient is lower in the L39 than in the L19 simulation. This is attributed to a stronger residual mean meridional circulation which is tantamount to a stronger upward transport velocity in the tropics.

4.2 $^{14}CO_2$

Regional results

The temporal evolution of the $^{14}CO_2$ mass due to nuclear weapon tests as simulated by the L39 model is depicted in Figure 13 for the total model atmosphere, troposphere, stratosphere, northern, and southern hemisphere. The structure of the L19 results is very similar and therefore not shown. After the initialisation in October 1963 the global $^{14}CO_2$ content in the atmosphere decreases with time, because $^{14}CO_2$ is absorbed by the oceans and the terrestrial biosphere. The decrease in time follows roughly an exponential curve with an e–folding time of nine years. The $^{14}CO_2$ content in the stratosphere decreases rapidly during the first year after the initialisation (by about 50%). It is dominated by the decrease of stratospheric $^{14}CO_2$ mass in the northern hemisphere. The e–folding times are 1.2 and 1.3 years for the L39 and L19 simulation, respectively. For the period October to December 1963 the e–folding times of the stratospheric northern hemisphere $^{14}CO_2$ mass differ significantly between both model runs. The values are 1.6 and 1.0 for the L39 and L19 simulation, respectively. That means the higher vertical resolution model L39 is more suited to preserve strong vertical tracer gradients. During the following months these gradients are smoothed and the e–folding times converge.

In the troposphere the modelled $^{14}CO_2$ mass increases during the first year by about 26%. During this time the transport of $^{14}CO_2$ from the stratosphere into the troposphere is stronger than the uptake in the oceans and in the terrestrial biosphere. The temporal variation of

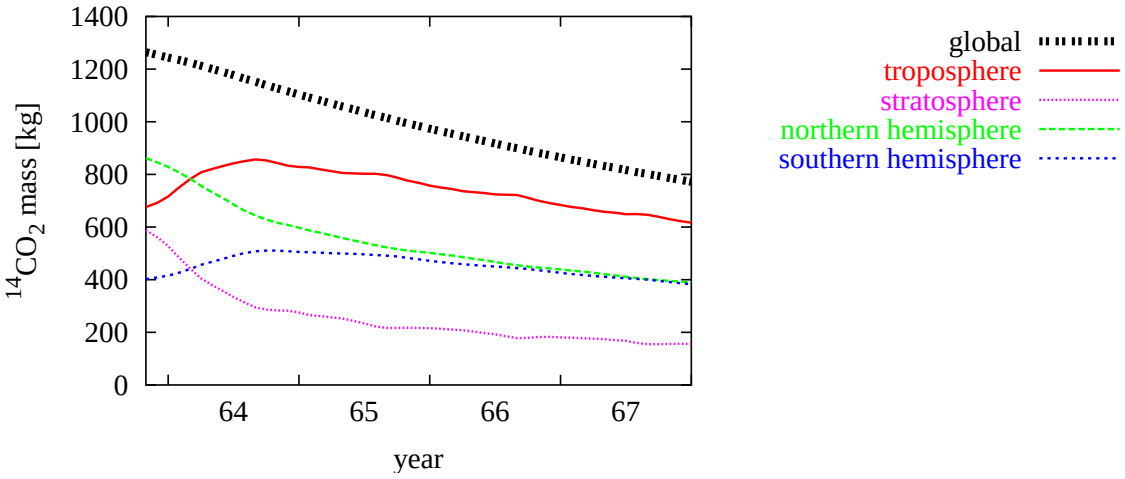

Figure 13: Temporal evolution of the $^{14}CO_2$ mass for selected regions of the atmosphere as modelled by L39.

stratospheric and tropospheric $^{14}CO_2$ masses can be explained by hemispheric differences of the seasonal variation of the tropopause height. In the global mean, the tropopause is higher in northern summer than in northern winter. Hence, the troposphere (stratosphere) encompasses a bigger (smaller) region and therefore the $^{14}CO_2$ mass during the summer months on the northern hemisphere is bigger (smaller) than during the winter months.

A comparison of the temporal evolution of the $^{14}CO_2$ mass in the northern and the southern hemisphere reveals that the fast decrease in the northern hemisphere can partly be explained by transport of $^{14}CO_2$ to the southern hemisphere. The hemispheric difference vanishes by the end of 1967. The annual mean interhemispheric exchange times are 0.83 and 0.86 years for the L39 and the L19 simulation, respectively. In either model simulation the interhemispheric exchange time shows a minimum in summer (see also *Kjellström et al.*, 2000). Later the $^{14}CO_2$ decrease in the atmosphere is a consequence of the uptake in the oceans and in the terrestrial biosphere.

$^{14}CO_2$ at the surface

In Figure 14 modelled and observed temporal evolutions of bomb produced $^{14}CO_2$ are displayed for selected surface stations as relative deviation from the natural background value in per mil (‰). *Kjellström et al.* (2000) have already shown that the initial $^{14}CO_2$ concentration used in the model simulation for October 1963 is higher than observed at all stations (see their Figure 16). As this deviation is only related to an erroneous initial $^{14}CO_2$ distribution, we have subtracted this offset in our comparison of modelled and observed $^{14}CO_2$ concentrations. Poleward of 28°N maximum $^{14}CO_2$ activity concentrations at the surface were observed in the late summer of 1963. Further south maximum concentrations occurred at later times, because the main input of bomb ^{14}C was in the northern hemisphere stratosphere. The observed

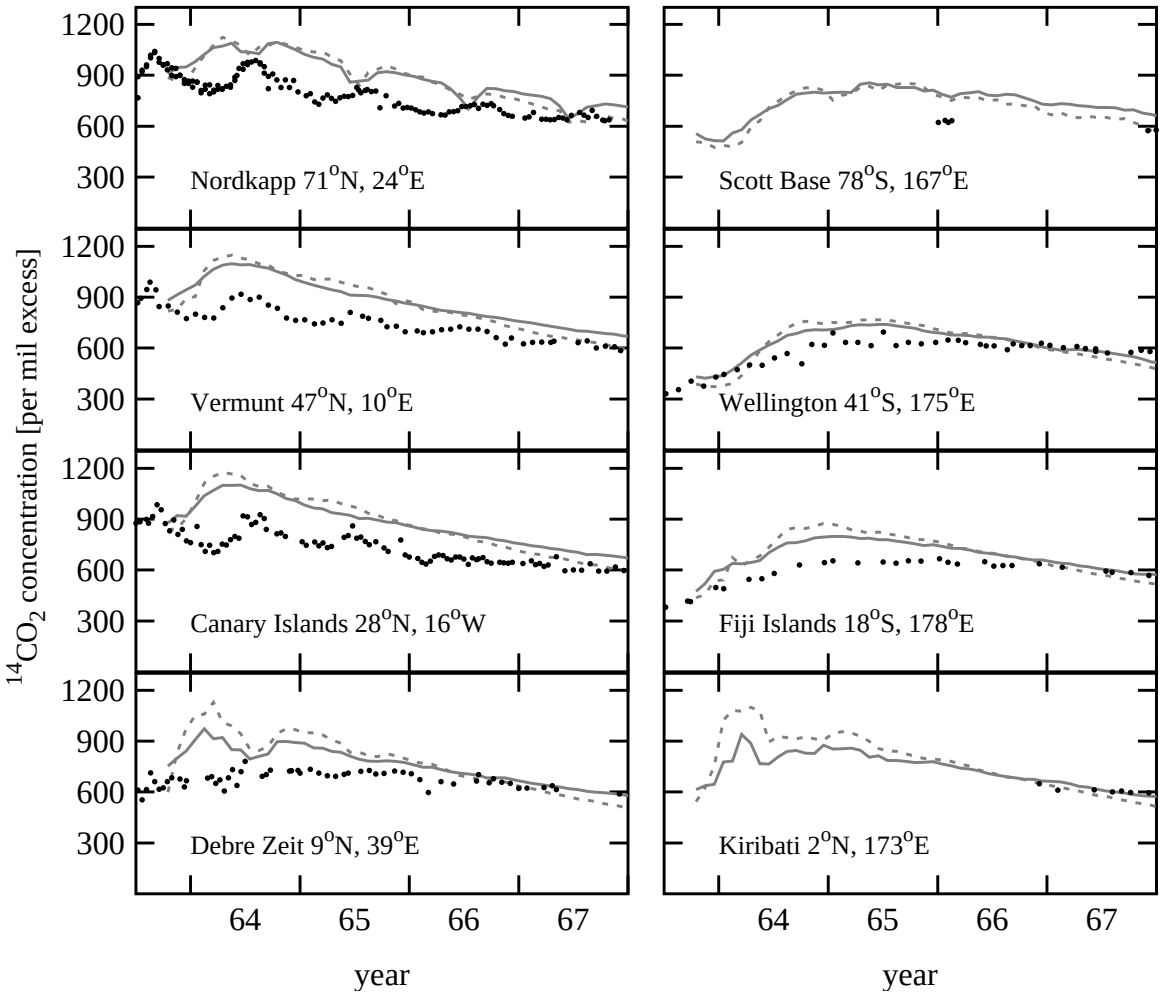

Figure 14: Observed (dots) and modelled (L39 grey line; L19 dashed) temporal evolution of the monthly mean $^{14}CO_2$ concentration at selected surface stations.

temporal difference of the occurrence of maximum $^{14}CO_2$ concentrations between Nordkapp and Wellington is 1.5 years. Later the concentration decreased at all stations, because nuclear test series had ended, and $^{14}CO_2$ was taken up by oceans and the terrestrial biosphere.

Compared to the observations the maximum concentrations at the surface in the model results occur at an earlier time and the concentration maximum is higher than observed. This overestimation can only be explained by a too strong downward transport in the initial stage of both model simulations. As air masses of northern hemispheric origin get mixed into the southern hemisphere with an interhemispheric exchange time of less than one year in both models (see above), the overestimated downward transport in northern hemisphere midlatitudes therefore also contributes to the southern hemispheric surface concentrations and leads to an overestimation of the $^{14}CO_2$ surface concentration on the southern hemisphere. *Reithmeier and Sausen* (2001) substituted the semi–Lagrangian advection scheme of ECHAM4 by a Lagrangian module and simulated the transport of $^{14}CO_2$. They found that the overestimated downward flux from the stratosphere into the troposphere is attributable to the numerical properties of the

semi–Lagrangian transport scheme and not to model dynamics. However, it is clearly visible that the values of the first concentration maximum are lower in the L39 simulation than in the L19 simulation, especially in mid- and lower latitudes of the northern hemisphere. This suggests that the downward transport is less overestimated in the higher vertical resolution model.

The $^{14}CO_2$ concentration decreases faster than observed at all surface stations in the L19 simulation. *Kjellström et al.* (2000) related this behavior to global sink terms, which are too strong. Figure 14 shows that this is also the case in the L39 simulation. However, in the L39 model the $^{14}CO_2$ concentration decreases more slowly at all stations in subsequent years than in the L19 simulation, e.g. at Nordkapp the observed e–folding time is 14.4 years, the L19 model simulates an e–folding time of 6.0 years and in the L39 simulation the e–folding time is 9.5 years. Also in this respect the L39 simulations is more in accord with the observations.

On the northern hemisphere at the stations Nordkapp, Vermunt, and Canary Islands strong seasonal variations of $^{14}CO_2$ with low values in spring and high values in summer were measured (Figure 14). They are more clearly analysed in Figure 15, where the long–term trend of the $^{14}CO_2$ concentration has been subtracted at each station from the respective temporal evolution shown in Figure 14. We approximated the long–term trend by assuming exponentially decreasing concentrations, starting with the first concentration maximum. The difference between the maximum concentration in 1963 and the subsequent minimum was about 160‰ at these stations. These fluctuations got weaker with time, because the $^{14}CO_2$ content in the northern stratosphere was depleted. They are due to seasonal variations in transport of $^{14}CO_2$ from the stratosphere. On the northern hemisphere this transport is strongest in spring and weakest in summer (*Appenzeller et al.*, 1996). It takes about half a year for this signal to reach the surface. At the southern hemisphere surface stations the seasonal variations had been weaker (see Figure 14), because the vertical gradient of the $^{14}CO_2$ concentration was much lower than on the northern hemisphere.

Compared to the observations the modelled seasonal variations at these stations show a lower amplitude and a phase lag (Nordkapp). The maximum surface concentration in northern hemispheric midlatitudes, observed in late summer 1964 at Nordkapp, Vermunt, and on the Canary Islands is modelled in the beginning of 1964. This model feature can again only be explained by a too strong downward transport from the stratosphere especially in midlatitudes in the initial stage of the simulation.

$^{14}CO_2$ is coupled with the global carbon cycle and therefore undergoes the same variations as CO_2. The exchange between the atmosphere and the terrestrial biosphere varies with time according to seasonal variations of plant growth. As a result, maximum CO_2 concentrations are observed in late winter and minimum CO_2 concentration in late summer with an amplitude of about 6 ppmv. In our model simulations we did not include seasonal variations of the $^{14}CO_2$

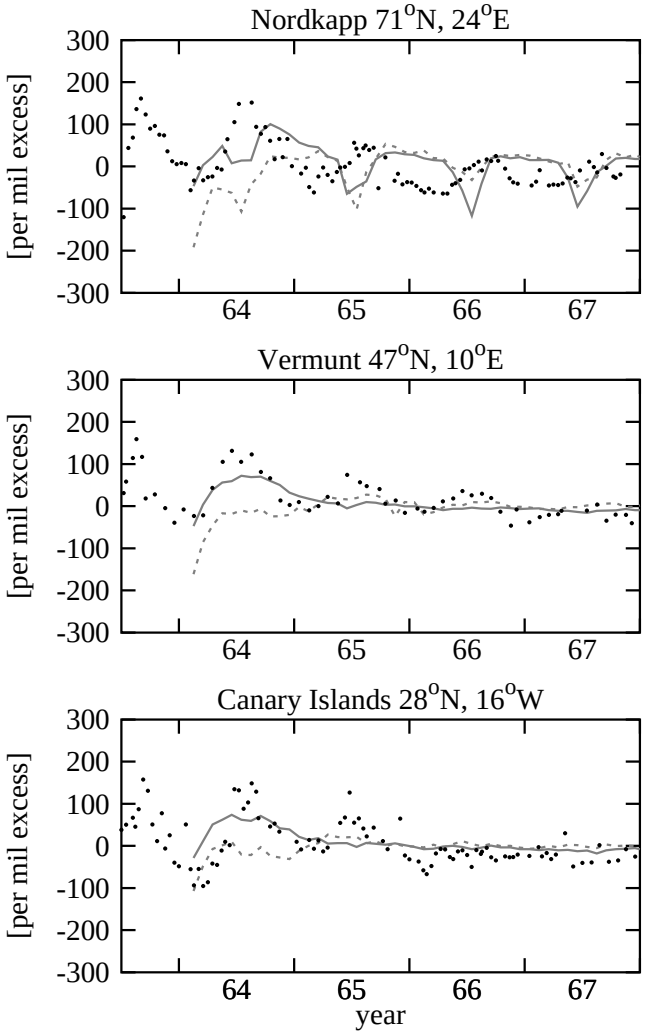

Figure 15: Observed (dots) and modelled (L39 grey line; L19 dashed) seasonal deviations from the long–term trend of the $^{14}CO_2$ concentration at the stations Nordkapp, Vermunt, and on the Canary Islands.

exchange between the atmosphere and the land biosphere, because they are negligible small: With a standard mixing ratio $^{14}CO_2/^{12}CO_2$ of 1.176 pptv the amplitude of the seasonal $^{14}CO_2$ cycle would be 7×10^{-18} mole/mole (compare with Figure 3). Thus, this simplification cannot explain the difference between observed and modelled seasonal $^{14}CO_2$ variations. Consequently, the $^{14}CO_2$ variation is dominated by seasonal variations of the downward transport from the stratosphere as well as fluctuations in horizontal transport of $^{14}CO_2$.

During the first year after the initialisation of $^{14}CO_2$ the seasonal variations calculated by the L39 model are more in accord with the observations than those simulated with L19. In subsequent years hardly any seasonal variations are visible at Vermunt and on the Canary Islands, and the modelled fluctuations are rather similar.

$^{14}CO_2$ vertical distribution

Figure 16 shows the temporal evolution of observed and modelled vertical profiles of the zonal mean $^{14}CO_2$ mixing ratio at 31°N. In autumn 1963 the maximum $^{14}CO_2$ mixing ratio is observed at 21 km altitude. The modelled maximum is about 2 km higher in the L39 simulation and its value is about 25% lower, whereas the L19 simulation captures the height of the initial $^{14}CO_2$ maximum, but the value is about 30% lower than observed. This discrepancy between

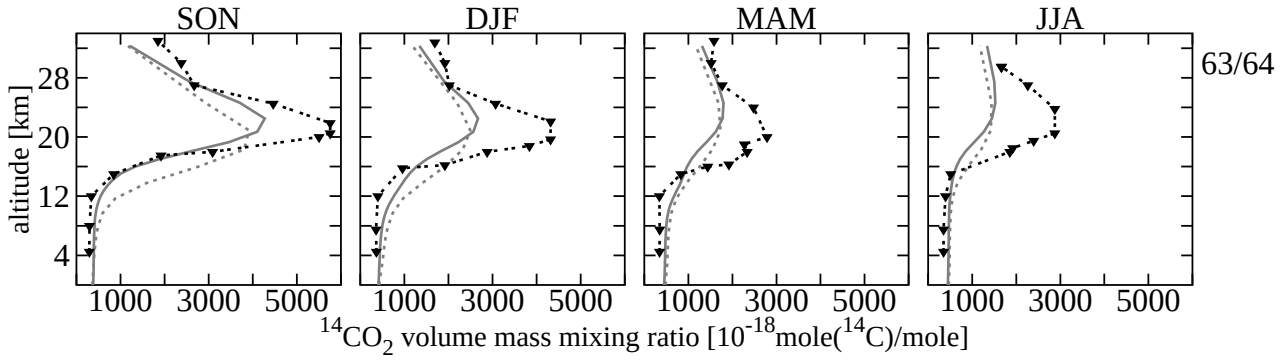

Figure 16: Modelled (L39 grey line; L19 dashed grey line) and observed (triangles) profiles of the excess $^{14}CO_2$ mixing ratio in autumn, winter, spring, and summer at 31°N in the years 1963 to 1964.

observations and model results is due to the fact that both models are started in October 1963 and the modelled profiles show the mean value of October and November, whereas the observations show the quarterly mean of September, October and November, with highest values observed in September. In the period autumn 1963 to summer 1964 the modelled maximum $^{14}CO_2$ concentrations are reduced by about 65%. The observed maximum decreases by 50%. Until autumn 1964 it is shifted upward by about 3 km in the model simulations due to the sink at the surface. In general the modelled values in the stratosphere are about 1.5 to 2 times lower than observed. Also in this figure it can be noticed, that the downward transport of $^{14}CO_2$ in the L39 model is weaker in the initial stage of the simulation, and the sharp concentration gradient at the tropopause is better maintained (see SON 63/64 in Figure 16) than in the L19 simulation. Hence, the L39 model simulation of $^{14}CO_2$ is more in accord with observations.

The modelled downward transport of $^{14}CO_2$ in the first months after the initialisation is stronger than observed, and the strong vertical concentration gradient above the tropopause is not maintained by the models to the same extent than observed. The reasons for this shortcoming are the downward transport which is too strong especially in midlatitudes, and a tropopause which is higher than observed (Figure 17). Figure 17 shows zonal means of the thermally defined tropopause pressure for all seasons determined from L39 and L19 results and from ECMWF data (see *World Meteorological Organization*, 1986, for the thermal definition of the tropopause). The modelled tropopause pressure is lower than observed at all latitudes and during all seasons. The difference between model results and observations is greatest at higher latitudes, e.g. on the northern hemisphere in autumn the observed tropopause pressure increases from 260 to

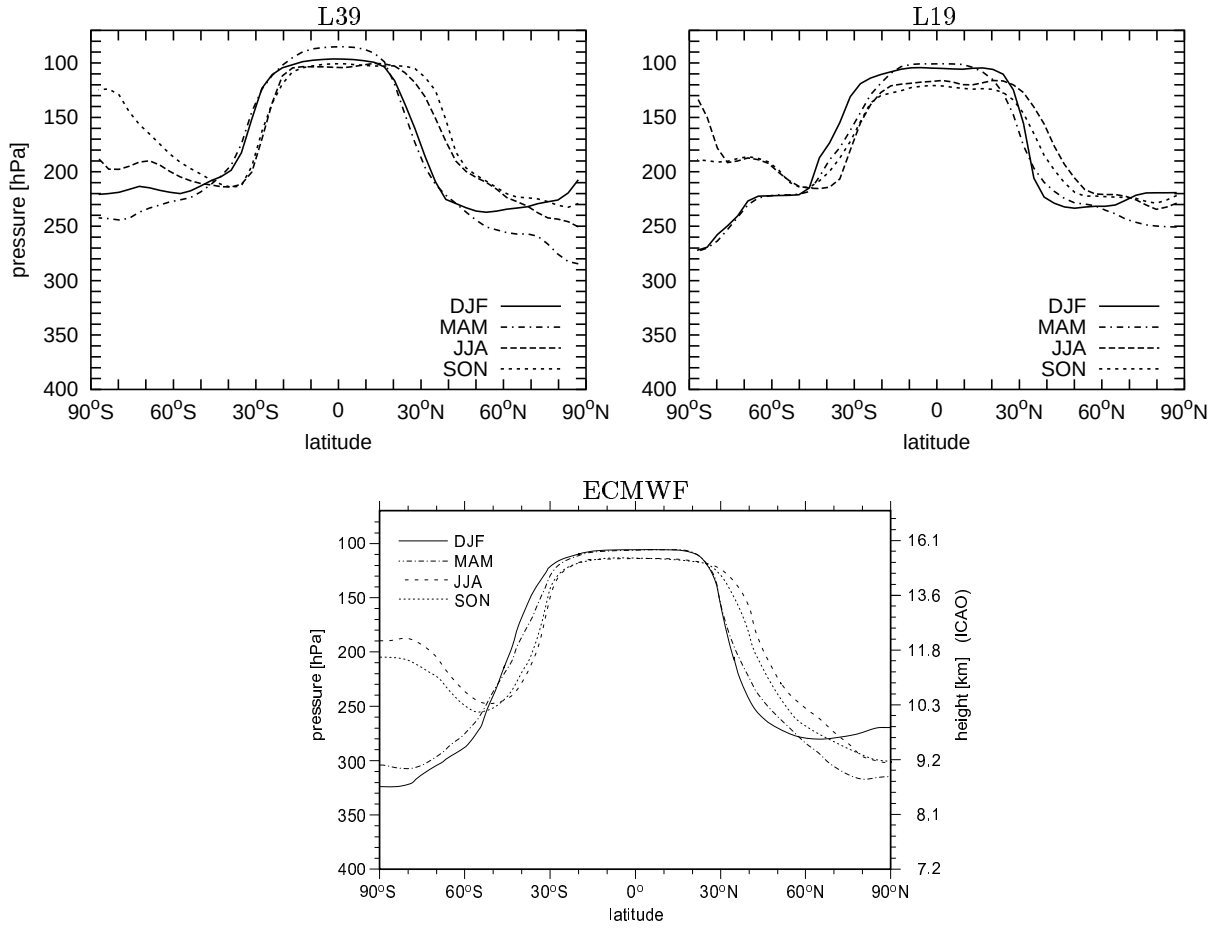

Figure 17: Modelled (L39: top left; L19: top right) and observed (ECMWF: bottom) zonal mean tropopause pressure for DJF, MAM, JJA, and SON. Unit: hPa.

300 hPa between 60° and 90°N, L39 model values increase from 230 to 240 hPa and the L19 tropopause pressure is about 230 hPa. This deviation is attributable to the cold bias in the lower stratosphere of both models. As a consequence, bomb produced $^{14}CO_2$ has been initialised partly in the troposphere where vertical transport and mixing is significantly higher than in the stratosphere. If this fraction had also been initialised in the stratosphere, it would have been transported much slower towards the surface. Hence, $^{14}CO_2$ surface concentrations would have been lower.

5 Summary and Conclusions

The impact of an increased vertical resolution on the transport and distribution of the passive tracers $^{14}CO_2$ and SF_6 has been investigated by means of numerical model simulations with two versions of ECHAM4 with the top level centred at 10 hPa and different vertical resolution: the standard model with 19 model layers and a higher resolution version with 39 layers. Both

models are able to reproduce the observed SF_6 concentrations in the troposphere. Only in the mid– and higher latitudes of the stratosphere they simulate higher mixing ratios than observed. In the lower latitudes of the stratosphere the modelled SF_6 mixing ratios are in good agreement with observations. L39 generally calculates higher stratospheric mixing ratios than L19, and the difference increases with altitude. This difference between the modelled profiles has been attributed to the residual mean meridional circulation, which is stronger in L39 than in L19. The deviation of the model results from the observed vertical profiles is due partly to the relatively coarse horizontal resolution which causes stronger horizontal mixing also into higher latitudes (i.e. the polar vortex) and partly to the initialisation of SF_6 with a globally constant concentration. These findings are confirmed by the vertical gradient of mean age calculated from the SF_6 distribution, which is weaker in the L39 than in the L19 simulation. A lower vertical gradient of the mean age is caused by a stronger residual mean meridional circulation. A stronger mean meridional circulation is tantamount to a higher upward transport velocity in the tropics.

The comparison of modelled $^{14}CO_2$ surface concentrations and vertical profiles with observations has shown that an increased vertical resolution in the climate model ECHAM4 reduces the strength of stratosphere troposphere exchange. L39 is more able to capture and maintain strong vertical gradients in tracer concentrations than L19. However, compared to observations the downward transport is too strong also in the L39 simulation.

One might suspect that the model dynamics is responsible for the excessive downward transport. However, *Reithmeier and Sausen* (2001) showed that this is not the case. They simulated the transport of $^{14}CO_2$ with a Lagrangian advection model coupled to ECHAM4. They found that the overestimated downward flux from the stratosphere to the troposphere is rather due to the numerical properties of the semi-Lagrangian transport scheme than due to incorrect model dynamics. Improvements with respect to the numerical properties of the semi–Lagrangian advection scheme could possibly be achieved by further increasing both the horizontal and the vertical resolution (*Rasch and Williamson*, 1990; *Rasch and Lawrence*, 1998).

Another possible influence factor, which has to be studied is the cold bias in the lower polar stratosphere of ECHAM4. Improvements with respect to the temperature structure would directly improve the location of the tropopause. One could suggest that the cold bias might partly be a reason for the too strong downward transport. *Land et al.* (1999) compared the residual mean meridional mass flux simulated by the two model versions, and calculated from ECMWF reanalysis (ERA) data. However, they did not find any systematic relationship between cold bias and residual mean meridional mass flux. The annual mean residual mean meridional mass flux calculated from ERA data is weaker on the southern hemisphere than the modelled mass flux. On the northern hemisphere the observed residual mass flux is slightly stronger than in the L19 results, but somewhat weaker than in the L39 results.

Acknowledgments: The authors are grateful to Ingeborg Levin from Institut für Umweltphysik, University of Heidelberg, Heidelberg, and Manfred Maiss from Max–Planck–Institut für Chemie, Mainz, for providing SF_6-data. G. Hoffmann from Laboratoire de Climat et de l'Environnement, Gif-sur-Yvette, France, provided the $^{14}CO_2$ surface module. We also thank Thomas Reichler for providing the zonal mean tropopause pressure calculated from ECMWF data. We are much indebted to Erik Kjellström from Department of Meteorology, Stockholm University, Stockholm, Claudia Timmreck, and Martin Schultz both from Max–Planck–Institut für Meteorologie, Hamburg, for their constructive suggestions on a former version of this paper. A large part of this work was carried out during the first author's stay at the Institut für Physik der Atmosphäre, DLR Oberpfaffenhofen.

References

Appenzeller, C., Holton, J. and Rosenlof, K. 1996. Seasonal variation of mass transport across the tropopause. *J. Geophys. Res.* **101**, 15071–15078.

Austin, J., Butchart, N. and Swinbank, R. 1997. Sensitivity of ozone and temperature to vertical resolution in a GCM with coupled stratospheric chemistry. *Q. J. R. Meteorol. Soc.* **123**, 1405–1431.

Boville, B. 1991. Sensitivity of simulated climate to model resolution. *J. Climate* **4**, 469–485.

Denning, A. et al. 1999. Three-dimensional transport and concentration of SF_6 – A model intercomparison study (TransCom 2). *Tellus* **51 B**, 226–297.

Feichter, J. and Lohmann, U. 1997. The atmospheric sulfur cycle in ECHAM-4 and its impact on the shortwave radiation. *Climate. Dyn.* **13**, 235–246.

Geller, L., Elkins, J., Lobert, J., Clarke, A., Hurst, D., Butler, J. and Myers, R. 1997. Tropospheric SF_6: Observed latitudinal distribution and trends, derived emissions and interhemispheric exchange time. *Geophys. Res. Lett.* **24**, 675–678.

Hall, T. and Plumb, R. 1994. Age as a diagnostic of stratospheric transport. *J. Geophys. Res.* **99**, 1059–1070.

Hall, T. and Waugh, D. 1997. Timescales for the stratospheric circulation derived from tracers. *J. Geophys. Res.* **102**, 8991–9001.

Hall, T. and Waugh, D. 1998. Influence of nonlocal chemistry on tracer distributions – Inferring the mean age of air from SF_6. *J. Geophys. Res.* **103**, 13327–13336.

Hall, T., Waugh, D., Boering, K. and Plumb, R. 1999. Evaluation of transport in stratospheric models. *J. Geophys. Res.* **104**, 18815–18839.

Harnisch, J., Borchers, R., Fabian, P. and Maiss, M. 1996. Tropospheric trends for CF_4 and C_2F_6 since 1982 derived from SF_6 dated stratospheric air. *Geophys. Res. Lett.* **23**, 1099–1102.

Harnisch, J., Bischof, W., Borchers, R., Fabian, P. and Maiss, M. 1998. A stratospheric excess of CO_2 – due to tropical deep convection?. *Geophys. Res. Lett.* **25**, 63–66.

Hesshaimer, V. and Levin, I. 2000. Revision of the stratospheric bomb $^{14}CO_2$ inventory. *J. Geophys. Res.* **105**, 11641–11658.

Hesshaimer, V., Heimann, M. and Levin, I. 1994. Radiocarbon evidence for a smaller oceanic carbon dioxide sink than previously believed. *Nature* **370**, 201–203.

Holton, J. 1986. Meridional distribution of stratospheric tracer constituents. *J. Atmos. Sci.* **43**, 1238–1242.

Johnston, H. 1989. Evaluation of excess carbon 14 and strontium 90 data for suitability to test two–dimensional stratospheric models. *J. Geophys. Res.* **94**, 18485–18493.

Kinnison, D., Johnston, H., Weisenstein, D. and Yue, G. 1993. Radionuclides as exotic tracers. In: *The Atmospheric Effects of Stratospheric Aircraft: Report of the 1992 Models and Measurements Workshop* (ed. M. Prather and E. Remsberg). Vol. III–Special Diagnostic Studies, pp. I–1–I–90.

Kjellström, E., Feichter, J. and Hoffmann, G. 2000. Transport of SF_6 and $^{14}CO_2$ in ECHAM4. *Tellus* **52 B**, 1–18.

Ko, M., Sze, N., W.-C.Wang, Shia, G., Goldman, A., F.J. Murcray, D. M. and Rinsland, C. 1993. Atmospheric sulfur hexafluoride: Sources, sinks, and greenhouse warming. *J. Geophys. Res.* **98**, 10499–10507.

Land, C., Ponater, M., Sausen, R. and Roeckner, E. 1999. The ECHAM4/L39(DLR) GCM – Technical description and model climatology. DLR–Forschungsbericht 1999–31, Deutsches Zentrum für Luft– und Raumfahrt Oberpfaffenhofen, Germany, 45 pp, ISSN 1434-8454.

Levin, I. and Hesshaimer, V. 1996. Refining of atmospheric transport model entries by the globally observed passive tracer distributions of ^{85}krypton and sulfur hexafluoride (SF_6). *J. Geophys. Res.* **101**, 16745–16755.

Lindzen, R. and Fox-Rabinovitz, M. 1989. Consistent vertical and horizontal resolution. *Mon. Wea. Rev.* **117**, 2575–2583.

Lohmann, U. and Roeckner, E. 1996. Design and performance of a new cloud microphysics scheme developed for the ECHAM general circulation model. *Climate. Dyn.* **12**, 557–572.

Maiss, M., Steele, L., Francey, R., Fraser, P., Langenfelds, R., Trivett, N. and Levin, I. 1996. Sulfur hexafluoride – A powerful new atmospheric tracer. *Atmos. Environ.* **30**, 1621–1629.

Manzini, E. and Feichter, J. 2000. Simulation of the SF_6 tracer with the middle atmosphere MAECHAM4 model: Aspects of the large–scale transport. *J. Geophys. Res.* **104**, 31097–31108.

Marshall, S., Roads, J. and Oglesby, R. 1997. Effects of resolution and physics on precipitation in the NCAR Community Climate Model. *J. Geophys. Res.* **102**, 19529–19541.

Nydal, R. and Lövseth, K. 1983. Tracing bomb ^{14}C in the atmosphere 1962–1980. *J. Geophys. Res.* **88**, 3621–3642.

Olga, P., Persson, G. and Warner, T. 1991. Model generation of spurious gravity waves due to inconsistency of the vertical and horizontal resolution. *Mon. Wea. Rev.* **119**, 917–935.

Patra, P., Lal, S., Subbaraya, B., Jackman, C. and Rajaratnam, P. 1997. Observed vertical profile of sulphur hexafluoride (SF_6) and its atmospheric applications. *J. Geophys. Res.* **102**, 8855–8859.

Pope, V., Pamment, J., Jackson, D. and Slingo, A. 2001. The representation of water vapour and its dependence on vertical resolution in the Hadley Centre Climate model. *J. Climate* **in press**.

Rasch, P. and Lawrence, M. 1998. Recent development in transport methods at NCAR. In: *MPI Workshop on conservative transport schemes* (ed. B. Machenhauer). Report No. 265, pp. 65–75, Hamburg, Germany, Max–Planck–Institut für Meteorologie.

Rasch, P. and Williamson, D. 1990. Computational aspects of moisture transport in global models of the atmosphere. *Q. J. R. Meteorol. Soc.* **116**, 1071–1090.

Ravishankara, A., Solomon, S., Turnipseed, A. and Warren, R. 1993. Atmospheric lifetimes of long-lived halogenated species. *Science* **259**, 194–199.

Reithmeier, C. and Sausen, R. 2001. Attila – Atmospheric tracer transport in a Lagrangian model. *Tellus* **submitted**, Also available as DLR–IPA Report No. 141, ISSN 0943–4771.

Roeckner, E. et al. 1992. Simulation of the present–day climate with the ECHAM model: Impact of model physics and resolution. Report No. 93, Max–Planck–Institut für Meteorologie, Hamburg, Germany, 171 pp.

Roeckner, E. et al. 1996. The atmospheric general circulation model ECHAM–4: Model description and simulation of present–day climate. Report No. 218, Max–Planck–Institut für Meteorologie, Hamburg, Germany, 90 pp.

Roeckner, E., Bengtsson, L., Feichter, J., Lelieveld, J. and Rodhe, H. 1999. Transient climate change simulations with a coupled atmosphere–ocean GCM including the tropospheric sulfur cycle. *J. Climate* **12**, 737–754.

Sausen, R., Feneberg, B. and Ponater, M. 1997. Climatic impact of aircraft induced ozone changes. *Geophys. Res. Lett.* **24**, 1203–1206.

Schmidt, U. and Khedim, A. 1991. In situ measurements of carbon dioxide in the winter Arctic vortex and at midlatitudes: An indicator of the "age" of stratospheric air. *Geophys. Res. Lett.* **18**, 763–766.

Senior, C. 1995. The dependence of climate sensitivity on the horizontal resolution of a GCM. *J. Climate* **8**, 2860–2880.

Shia, R.-L., Ko, M., Zou, M. and Kotamarthi, V. 1993. Cross–tropopause transport of excess ^{14}C in a two–dimensional model. *J. Geophys. Res.* **98**, 18599–18606.

Simmons, A., Burridge, D., Jarraud, M., Girard, C. and Wergen, W. 1989. The ECMWF medium–range prediction models: Development of the numerical formulations and the impact of increased resolution. *Meteorol. Atmos. Phys.* **40**, 28–60.

Stendel, M. and Roeckner, E. 1998. Impacts of horizontal resolution on simulated climate statistics in ECHAM4. Report No. 253, Max–Planck–Institut für Meteorologie, Hamburg, Germany, 57 pp.

Timmreck, C., Graf, H.-F. and Feichter, J. 1999. Simulation of Mt. Pinatubo aerosol with the Hamburg climate model. *Theor. Appl. Climatol.* **62**, 85–108.

Tompkins, A. and Emanuel, K. 2000. The vertical–resolution sensitivity of simulated equilibrium tropical temperature and water–vapour profiles. *Q. J. R. Meteorol. Soc.* **126**, 1219–1238.

Tsuyuki, T. 1994. Impacts of increased vertical resolution in the stratosphere on dynamical extended–range forecasts. *J. Meteor. Soc. Japan* **72**, 795–810.

Upstillgoddard, R. and Wilkins, C. 1998. The potential of SF_6 as a geothermal tracer. *Water Res.* **29**, 1065–1068.

Volk, C., Elkins, J., Fahey, D., Dutton, G., Gilligan, J., Loewenstein, M., Podolske, J., Chan, K. and Gunson, M. 1997. Evaluation of source gas lifetimes from stratospheric observations. *J. Geophys. Res.* **102**, 25543–25564.

Waugh, D. et al. 1997. Three–dimensional simulations of long–lived tracers using winds from MACCM2. *J. Geophys. Res.* **102**, 21493–21513.

Williamson, D. and Rasch, P. 1989. Two–dimensional semi–Lagrangian transport with shape–preserving interpolation. *Mon. Wea. Rev.* **117**, 102–129.

Williamson, D. and Rasch, P. 1994. Water vapor transport in the NCAR CCM2. *Tellus* **46 A**, 34–51.

Williamson, D., Kiehl, J. and Hack, J. 1995. Climate sensitivity of the NCAR Community Climate Model (CCM2) to horizontal resolution. *Climate. Dyn.* **11**, 377–397.

World Meteorological Organization 1986. Atmospheric ozone 1985. Global Ozone Research and Monitoring Project Report No. 16, Geneva, Switzerland.

MPI-Report-Reference: *Reprinted in

Report 1-276 Please order the reference list from MPI for Meteorology, Hamburg

---

Report No. 277
September 1998

Interannual to Decadal Variability in the Tropical Atlantic
Dietmar Dommenget, Mojib Latif
* Journal of Climate, 1998 (submitted)

Report No. 278
October 1998

Application of a grid-scale lateral discharge model in the BALTEX region
Stefan Hagemann, Lydia Dümenil
* Nordic Hydrology, 30 (3), 209-230, 1999

Report No. 279
October 1998

Cyclostationary Circulation Estimation with a Global Ocean Assimilation System
Detlev Müller, Ralf Giering, Uwe Mikolajewicz, Ernst Maier-Reimer

Report No. 280
October 1998

A coarse grid three dimensional global inverse model of the atmospheric transport
1. Adjoint Model and Jacobian Matrix
2. Inversion of the transport of CO_2 in the 1980s
Thomas Kaminski, Martin Heimann, Ralf Giering
* Journal of Geophysical Research, 1998 (submitted)

Report No. 281
November 1998

Paleonutrient Data Analysis of the Glacial Atlantic using an Adjoint Ocean General Circulation Model
Arne M. E. Winguth, David Archer, Ernst Maier-Reimer, Uwe Mikolajewicz
* AGU Geophysical Monograph Series, Vol. 114, 171-183, 1999

Report No. 282
November 1998

The Effect of Environmental Conditions on Volcanic Plume Rise
Hans-F. Graf, Michael Herzog, Josef M. Oberhuber, Christiane Textor
* Journal of Geophysical Research, 1998 (submitted)

Report No. 283
December 1998

Model Simulations of the Changing Distribution of Ozone and its Radiative Forcing of Climate:
Past, Present and Future
Geert-Jan Roelofs, Jos Lelieveld, Johann Feichter

Report No. 284
December 1998

Predicting the Number of Cloud Droplets in the ECHAM GCM
Ulrike Lohmann, Johann Feichter, Catherine C. Chuang, Joyce E. Penner
* Journal of Geophysical Research - Atmospheres, 1998 (accepted)

Report No. 285
December 1998

The Role of Ocean Dynamics for Low-Frequency Fluctuations of the NAO in a Coupled Ocean-Atmosphere GCM
Michael Christoph, Uwe Ulbrich, Josef M. Oberhuber, Erich Roeckner

Report No. 286
January 1999

Formation of nitrous acid: Parameterisation and comparison with observations
Gerhard Lammel

Report No. 287
Februar 1999

Natürliche Senken und Quellen des atmosphärischen Kohlendioxids: Stand des Wissens und Optionen des Handelns
Martin Heimann, Christine Weber, Jan C. Duinker, Arne Körtzinger, Ludger Mintrop, Nina Buchmann, Ernst-Detlef Schulze, Michaela Hein, Alberte Bondeau, Wolfgang Cramer, Marcus Lindner, Gerd Esser

Report No. 288
March 1999

Large-eddy simulation of a nocturnal stratocumulus-topped marine atmospheric boundary layer:
An uncertainty analysis
Andreas Chlond, Andreas Wolkau
Boundary-Layer Meteorology, 1999 (submitted)

Report No. 289
March 1999

Derivation of global GCM boundary conditions from 1 km land use satellite data
Stefan Hagemann, Michael Botzet, Lydia Dümenil, Bennert Machenhauer

Report No. 290
June 1999
A nonlinear impulse response model of the coupled carbon cycle-ocean-atmosphere climate system
Georg Hooss, Reinhard Voss, Klaus Hasselmann, Ernst Maier-Reimer, Fortunat Joos

Report No. 291
June 1999
Rapid algorithms for plane-parallel radiative transfer calculations
Vassili Prigarin

Report No. 292
June 1999
Oceanic Control of Decadal North Atlantic Sea Level Pressure Variability in Winter
Mojib Latif, Klaus Arpe, Erich Roeckner
* Geophysical Research Letters, 1999 (submitted)

Report No. 293
July 1999
A process-based, climate-sensitive model to derive methane emissions from natural wetlands: Application to 5 wetland sites, sensitivity to model parameters and climate
Bernadette P. Walter, Martin Heimann
* Global Biogeochemical Cycles, 1999 (submitted)

Report No. 294
August 1999
Possible Changes of $\delta^{18}O$ in Precipitation Caused by a Meltwater Event in the North Atlantic
Martin Werner, Uwe Mikolajewicz, Georg Hoffmann, Martin Heimann
* Journal of Geophysical Research - Atmospheres, 105, D8, 10161-10167, 2000

Report No. 295
August 1999
Borehole versus Isotope Temperatures on Greenland: Seasonality Does Matter
Martin Werner, Uwe Mikolajewicz, Martin Heimann, Georg Hoffmann
* Geophysical Research Letters, 27, 5, 723-726, 2000

Report No. 296
August 1999
Numerical Modelling of Regional Scale Transport and Photochemistry directly together with Meteorological Processes
Bärbel Langmann
* Atmospheric Environment, 34, 3585-3598, 2000

Report No. 297
August 1999
The impact of two different land-surface coupling techniques in a single column version of the ECHAM4 atmospheric model
Jan-Peter Schulz, Lydia Dümenil, Jan Polcher
* Journal of Applied Meteorology, 40, 642-663, 2001

Report No. 298
September 1999
Long-term climate changes due to increased CO_2 concentration in the coupled atmosphere-ocean general circulation model ECHAM3/LSG
Reinhard Voss, Uwe Mikolajewicz
* Climate Dynamics, 17, 45-60, 2000

Report No. 299
October 1999
Tropical Stabilisation of the Thermohaline Circulation in a Greenhouse Warming Simulation
Mojib Latif, Erich Roeckner
* Journal of Climate, 1999 (submitted)

Report No. 300
October 1999
Impact of Global Warming on the Asian Winter Monsoon in a Coupled GCM
Zeng-Zhen Hu, Lennart Bengtsson, Klaus Arpe
* Journal of Geophysical Research-Atmosphere, 105, 4607-4624, 2000

Report No. 301
December 1999
Impacts of Deforestation and Afforestation in the Mediterranean Region as Simulated by the MPI Atmospheric GCM
Lydia Dümenil Gates, Stefan Ließ

Report No. 302
December 1999
Dynamical and Cloud-Radiation Feedbacks in El Niño and Greenhouse Warming
Fei-Fei Jin, Zeng-Zhen Hu, Mojib Latif, Lennart Bengtsson, Erich Roeckner
* Geophysical Research Letter, 28, 8, 1539-1542, 2001

Report No. 303
December 1999
The leading variability mode of the coupled troposphere-stratosphere winter circulation in different climate regimes
Judith Perlwitz, Hans-F. Graf, Reinhard Voss
* Journal of Geophysical Research, 105, 6915-6926, 2000

Report No. 304
January 2000
Generation of SST anomalies in the midlatitudes
Dietmar Dommenget, Mojib Latif
* Journal of Climate, 1999 (submitted)

Report No. 305
June 2000
Tropical Pacific/Atlantic Ocean Interactions at Multi-Decadal Time Scales
Mojib Latif
* Geophysical Research Letters, 2000 (submitted)

Report No. 306
June 2000
On the Interpretation of Climate Change in the Tropical Pacific
Mojib Latif
* Journal of Climate, 2000 (submitted)

Report No. 307
June 2000
Observed historical discharge data from major rivers for climate model validation
Lydia Dümenil Gates, Stefan Hagemann, Claudia Golz

Report No. 308
July 2000
Atmospheric Correction of Colour Images
of Case I Waters - a Review
of Case II Waters - a Review
D. Pozdnyakov, S. Bakan, H. Grassl
* Remote Sensing of Environment, 2000 (submitted)

Report No. 309
August 2000
A Cautionary Note on the Interpretation of EOFs
Dietmar Dommenget, Mojib Latif
* Journal of Climate, 2000 (submitted)

Report No. 310
September 2000
Midlatitude Forcing Mechanisms for Glacier Mass Balance Investigated Using General Circulation Models
Bernhard K. Reichert, Lennart Bengtsson, Johannes Oerlemans
* Journal of Climate, 2000 (accepted)

Report No. 311
October 2000
The impact of a downslope water-transport parameterization in a global ocean general circulation model
Stephanie Legutke, Ernst Maier-Reimer

Report No. 312
November 2000
The Hamburg Ocean-Atmosphere Parameters and Fluxes from Satellite Data (HOAPS):
A Climatological Atlas of Satellite-Derived Air-Sea-Interaction Parameters over the Oceans
Hartmut Graßl, Volker Jost, Ramesh Kumar, Jörg Schulz, Peter Bauer, Peter Schlüssel

Report No. 313
December 2000
Secular trends in daily precipitation characteristics: greenhouse gas simulation with a coupled AOGCM
Vladimir Semenov, Lennart Bengtsson

Report No. 314
December 2000
Estimation of the error due to operator splitting for micro-physical-multiphase chemical systems in meso-scale air quality models
Frank Müller
* Atmospheric Environment, 2000 (submitted)

Report No. 315
January 2001
Sensitivity of global climate to the detrimental impact of smoke on rain clouds
Hans-F. Graf, Daniel Rosenfeld, Frank J. Nober
* nur unter www.mpimet.mpg.de · Veröffentlichungen · MPI-Reports

Report No. 316 March 2001	**Lake Parameterization for Climate Models** Ben-Jei Tsuang, Chia-Ying Tu, Klaus Arpe
Report No 317 March 2001	**The German Aerosol Lidar Network:** **Methodology, Data, Analysis** J. Bösenberg, M. Alpers, D. Althausen, A. Ansmann, C. Böckmann, R. Eixmann, A. Franke, V. Freudenthaler, H. Giehl, H. Jäger, S. Kreipl, H. Linné, V. Matthias, I. Mattis, D. Müller, J. Sarközi, L. Schneidenbach, J. Schneider, T. Trickl, E. Vorobieva, U. Wandinger, M. Wiegner
Report No. 318 March 2001	**On North Pacific Climate Variability** Mojib Latif * Journal of Climate, 2001 (submitted)
Report No. 319 March 2001	**The Madden-Julian Oscillation in the ECHAM4 / OPYC3 CGCM** Stefan Liess, Lennart Bengtsson, Klaus Arpe * Climate Dynamics, 2001 (submitted)
Report No. 320 May 2001	**Simulated Warm Polar Currents during the Middle Permian** A. M. E. Winguth, C. Heinze, J. E. Kutzbach, E. Maier-Reimer, U. Mikolajewicz, D. Rowley, A. Rees, A. M. Ziegler * Paleoceanography, 2001 (submitted)
Report No. 321 June 2001	**Impact of the Vertical Resolution on the Transport of Passive Tracers in the ECHAM4 Model** Christine Land, Johann Feichter, Robert Sausen * Tellus, 2001 (submitted)

ISSN 0937-1060